DOE/MT/93006--T5

Technical Progress Report No.10

Investigation of Heat Transfer and Combustion in the Advanced Fluidized Bed Combustor (FBC)

to

U.S. Department of Energy
Pittsburgh Energy Technology Center
P.O. Box 10940, MS 921-118
Pittsburgh, PA 15236-0940

for

Project No: DE-FG22-93MT93006

by

Dr. Seong W. Lee, Principal Investigator

Morgan State University
School of Engineering
Baltimore, MD 21239
(phone) 410-319-3137

April 1996

SUMMARY

This technical report summarizes the research performed and progress achieved during the period of January 1, 1996 to march 31, 1996.

Numerical modeling and simulation on the gas velocity and pressure were performed to understand swirling, recirculating, turbulent flow in the test chamber. The flow pattern and the pressure profiles were predicted. At the bottom of the chamber, the velocity at the center is greater than that of the wall region. When the secondary air is injected into the chamber, gas velocity decreases rapidly but whole chamber achieves a swirling flow. The profiles show that the gas at the near wall region flows down to the bottom and flows up at the center region, and velocity at the center region increases up along the axis of the combustor chamber.

The pressure at the outer region near the wall is greater than that at the inner region near the axis. The pressure at the bottom is greater than that at the top region. The higher pressure zone is formed surrounding the secondary air flow into the center region.

The exploratory hot model was designed to better understand the combustion processes and the local heat transfer phenomena in the combustor chamber. Design and Fabrication of the exploratory hot model will be continued with an arrangement of the auxiliary subsystems. Instrumentation for the system test will be arranged with a computer-assisted data acquisition system.

TABLE OF CONTENTS

Section 1

Numerical Modeling and Simulation

1.1 Profiles of Gas Velocity and Pressure in the Combustor Chamber

The cold flow pattern in the swirling combustor chamber was simulated by using the Computational Fluid Dynamics code, Fluent [1], to determine the three velocity component profiles in three different directions: vertical direction (K), radial direction (J), tangential direction (I); and the static pressure profile in the chamber. In order to simulate the problem completely, the following basic procedures were carefully considered.

Using a numerical calculation procedure, the governing fluid flow equations, continuity and momentum equations in cylindrical coordinates are employed to determine the velocity and pressure in the combustion chamber. The continuity and three direction momentum equations are the following equations [1,2]: equation (1) through equation (10)

Continuity:

$$\frac{\partial \rho}{\partial t}+\frac{\partial(\rho u)}{\partial x}+\frac{1}{r}\frac{\partial(r\rho v)}{\partial r}+\frac{1}{r}\frac{\partial(\rho w)}{\partial \theta}=RSM \tag{1}$$

Axial Direction Momentum:

$$\begin{aligned}&\frac{\partial(\rho u)}{\partial t}+\frac{\partial(\rho uu)}{\partial x}+\frac{1}{r}\frac{\partial(r\rho vu)}{\partial r}+\frac{1}{r}\frac{\partial(\rho wu)}{\partial \theta}\\&=-\frac{\partial P}{\partial x}+\frac{\partial(\tau_{xx})}{\partial x}+\frac{1}{r}\frac{\partial(r\rho v)}{\partial r}+\frac{1}{r}\frac{\partial(\tau_{x\theta})}{\partial \theta}+\rho g_x+F_x\end{aligned} \tag{2}$$

Radial Direction Momentum:

$$\begin{aligned}&\frac{\partial(\rho v)}{\partial t}+\frac{\partial(\rho uv)}{\partial x}+\frac{1}{r}\frac{\partial(r\rho vv)}{\partial r}+\frac{1}{r}\frac{\partial(\rho wv)}{\partial \theta}\\&=-\frac{\partial p}{\partial r}+\frac{\rho w^2}{r}+\frac{\partial(\tau_{xr})}{\partial x}+\frac{1}{r}\frac{\partial(r\tau_{rr})}{\partial r}+\frac{1}{r}\frac{\partial(\tau_{r\theta})}{\partial \theta}-\frac{\tau_{\theta\theta}}{r}+\rho g_r+F_r\end{aligned} \tag{3}$$

Circumferential Direction Momentum:

$$\frac{\partial(\rho w)}{\partial t}+\frac{\partial(\rho uw)}{\partial x}+\frac{1}{r}\frac{\partial(r\rho vw)}{\partial r}+\frac{1}{r}\frac{\partial(\rho ww)}{\partial\theta} \tag{4}$$
$$=-\frac{1}{r}-\frac{\rho vw}{r}+\frac{\partial(\tau_{x\theta})}{\partial x}+\frac{1}{r^2}\frac{\partial(r^2\tau_{r\theta})}{\partial r}+\frac{1}{r}\frac{\partial(\tau_{\theta\theta})}{\partial\theta}+\rho g_\theta+F_\theta$$

where u is the axial velocity component, v is the radial velocity component, and w is the circumferential velocity component. The stress tensor in cylindrical coordinates is:

$$\tau_{xx}=2\mu\frac{\partial u}{\partial x}-\frac{2}{3}\mu\left(\frac{\partial u}{\partial x}+\frac{1}{r}\frac{\partial(rv)}{\partial r}\right)+\frac{1}{r}\frac{\partial w}{\theta} \tag{5}$$

$$\tau_{rr}=2\mu\frac{\partial v}{\partial r}-\frac{2}{3}\mu\left(\frac{\partial u}{\partial x}+\frac{1}{r}\frac{\partial(rv)}{\partial r}\right)+\frac{1}{r}\frac{\partial w}{\theta} \tag{6}$$

$$\tau_{\theta\theta}=2\mu\frac{1}{r}\frac{\partial w}{\partial\theta}+\frac{v}{r}-\frac{2}{3}\mu\left(\frac{\partial u}{\partial x}+\frac{1}{r}\frac{\partial(rv)}{\partial r}\right)+\frac{1}{r}\frac{\partial w}{\theta} \tag{7}$$

$$\tau_{xr}=\mu\frac{\partial u}{\partial r}+\frac{\partial v}{\partial x} \tag{8}$$

$$\tau_{x\theta}=\mu\frac{1}{r}\frac{\partial u}{\partial\theta}+\frac{\partial w}{\partial x} \tag{9}$$

$$\tau_{x\theta}=\mu\frac{1}{r}\frac{\partial u}{\partial\theta}+\frac{\partial w}{\partial x} \tag{10}$$

1.2 System Configuration

The solution process requires a geometry modeler, grid generator, and system configuration. The system was configured in 3-D cylindrical coordinates with uniform mesh grids. The combustor chamber was 36 inches in height and 10 inches in diameter. The

computation grid configuration is shown in Figure 1. There are a total of 12,136 grids in the system configuration, 41 pieces are in the tangential direction, I, 8 pieces are in the radial direction, J, and 37 pieces are in the vertical direction, K. Only three slices for the surfaces of the cylinder were shown in the Figure. They are bottom surface (K=1), top surface (K=37), and side wall surface (J=8).

1.3 Test Conditions

The test conditions and input boundary conditions are summarized in Table 1.

Table 1. Test Conditions for FLUENT simulation

Reactor diameter	inch	10
Reactor height	inch	36
top secondary nozzle	inch	24
bottom secondary nozzle	inch	12
Primary Air Flow Rate	ft^3/s	1.39
Gas Velocity at bottom	ft/s	2.55
Secondary Air Flow rate	ft^3/s	0.2323
Gas velocity at nozzle	ft/s	75.6
nozzle yam angle	degree	30
nozzle pitch angle	degree	0
temperature	°C	22
test pressure	atm	1
gas density	lb/ft^3	0.08

Since the swirling flow is a strong turbulence flow with anisotropic behaviors, the k-ε turbulence model is not suitable for this case[3]. The simplified Algebraic Stress Model (ASM) was selected and tested for the swirling turbulence flow simulation. The gas density was simplified to take the constant value 0.08 lb/ft^3. After 6340 interaction calculations, a good convergence was indicated for the gas flow profiles. The Reynold stress models

are presented in equations (11), (12), (13), and Table 2.

In the Reynolds averaging of the momentum equations, the velocity at a point is considered as a sum of the mean (time averaged) and fluctuating components:

$$u_i = \overline{u_i} + u_i \tag{11}$$

Substituting expressions of this form into the basic momentum balance (and dropping the overbar on the mean velocity, u) yields the ensemble-averaged momentum equations applied by FLUENT for predicting turbulent flows:

$$\frac{\partial(\rho u_i)}{\partial t} + \frac{\partial(\rho u_i u_j)}{\partial xj} = \frac{\partial}{\partial xj}\left(\mu\left[\frac{\partial u_i}{\partial xj} + \frac{\partial u_j}{\partial xi}\right] - \left(\frac{2}{3}\mu\frac{\partial u_i}{\partial xi}\right)\right) - \frac{\partial p}{\partial xi} + \rho_{gi} + F_i + \frac{\partial(\rho \overline{u_i' u_j'})}{\partial xj} \tag{12}$$

Equation (12) has the same form as the fundamental momentum balance with velocities now representing time-averaged (or mean-flow) values and the effect of turbulence incorporated through the "Reynolds stresses", $\rho \overline{u'_i u'_j}$. Note that $\overline{u'_i u'_j}$ is a symmetric second order tensor since:

$$\overline{u_i' u_j'} = \overline{u_j' u_i'} \tag{13}$$

and hence has six unique terms. The main task of turbulence models is to provide expressions or closure models that allow the evaluation of these correlations in terms of mean flow quantities. The turbulence closure models used in FLUENT are:

Table 2. Curvature-Related Source Terms in the RSM

ij	S_{ij}	D_{ij} algebraic	D_{ij} differential
xx	———	———	———
xr	$\rho \frac{v_\theta}{r} v_x' v_\theta'$	$-v_x' v_r' \frac{\mu_t}{r^2}$	$-B v_x' v_\theta'$
xθ	$-\rho \frac{v_\theta}{r} v_x' v_r'$	$-v_x' v_\theta' \frac{\mu_t}{r^2}$	$B v_x' v_r'$
rr	$2\rho \frac{v_\theta}{r} v_r' v_\theta'$	$-2(v_r'^2 - v_\theta'^2) \frac{\mu_t}{r^2}$	$-2B v_r' v_\theta'$
rθ	$\rho \frac{v_\theta}{r} (v_\theta'^2 - v_r'^2)$	$-4 v_r' v_\theta' \frac{\mu_t}{r^2}$	$B(v_r'^2 - v_\theta'^2)$
θθ	$-2\rho \frac{v_\theta}{r} v_r' v_\theta'$	$2(v_r'^2 - v_\theta'^2) \frac{\mu_t}{r^2}$	$2B v_r' v_\theta'$

$$B \equiv \left(\frac{1}{r^2}\partial_\theta \mu_t\right) + \frac{2\mu_t}{r^2}\partial_\theta$$

1.4 Simulation Results for Gas Flow Pattern in the Combustor Chamber

The simulation results are shown in Figures 2 through 15. Figure 2 shows the velocity-vectors at five levels. K=6, 12, 18, 24, and 30, and the scaling factor to be equal to 1 (Dimensionless). The details of the velocity-vectors for the seven levels are shown in Figures 7 through 11 (Figure 7 for level 6, Figure 8 for level 12, Figure 9 for level 18, Figure 10 for level 24, Figure 11 for level 30). Figure 3 shows the pressure profiles are shown in Figure 3 at six levels. K=6, 12, 18, 24, 30, and 33, and the scaling factor to be equal to 1 (Dimensionless). The

details of the pressure profiles for the six levels are shown in Figures 12 through 15 (Figure 12 for level 6, Figure 13 for level 12, Figure 14 for level 18, Figure 15 for level 24, Figure 16 for level 30, Figure 15 for level 33). Figure 4 and Figure 6 show a 2-D velocity-vector in slide plates I=2 and I=22. The pressure profiles in the same 2-D slides are shown in Figure 5.

1.4.1 The Flow Pattern

At the bottom of the chamber, the velocity at the center is greater than it is nearer the wall region. At the secondary air injection levels, K = 12 and K = 24 (see Figure 13 and Figure 15), the outside velocity is greater than at the center. In the level between the two secondary air injectors, K = 18 (see Figure 14), the outside velocity is reduced to less than the center velocity. At the top region (above the top secondary air injectors), the velocity increases from the wall to the center region.

At level K = 6 (see Figure 7), the velocity at the near wall is about 32 ft/s. By closing the center, it increases to 37 ft/s. However, in the center, it is reduced to about 20 ft/s.

At level K = 12 (see Figure 13), the velocity of the secondary air nozzle outlet is 60 ft/s. When the air is injected into the chamber, it decreases rapidly but the whole chamber achieves a swirling flow. The swirling velocity is about 4 ft/s at J = 6 radial position and is reduced in both directions, to the wall and to the center of the chamber. In the center, however, and behind the nozzle, there are some lesser velocities (about 20 ft/s).

It is more interesting to note Figure 9 which shows the details of velocity-vector at the 18 inch level. At the level place, the highest velocity is about 49 ft/s at the center region and is reduced to about 34 ft/s at the near wall region (see the color scales). However, the tangential velocity component is increased from the inner region to the outer region (see the arrow scales).

It is noted that velocity-vectors in Figure 4 and Figure 6 indicate the velocity profile in a vertical plate (I=2, and 22). Figure 4 is a front view of the profile, and Figure 6 is the side

view of the profile. The profiles clearly show that the gas at the near wall region flows down to the bottom and flows up at the center region, and the velocity at the center region increases up along the axis of the combustor (see the arrow scales in Figure 4). Two larger tangential velocities are fond at the secondary air injection levels (see arrow scales in Figure 6), The overall velocity in the chamber changes from 15.8 ft/s to 93.8 ft/s (see the color scales in the two Figures).

1.4.2 The Pressure Profiles

The overall static pressure profiles are shown in Figure 3 and Figure 5. The details for pressure profiles at each level are shown in Figure 12 through 15. In general, the pressure at the outer region near the wall is greater than that at the inner region near the axis; and the pressure at the bottom is greater than that at the top region. The pressure profiles for the vertical plate (I=2 and 22) are clearly shown in Figure 5. A negative pressure is formed at the top center region. The pressure is about -0.092 psi. We recognize that a lower pressure is always located at the chamber's center region and in the upper one. Since a higher velocity is always found at the center region, according to the Bernoulli equation, the increasing velocity is coming form pressure potential energy and is transferred into kinetic energy. It was noted that a higher pressure zone is formed surrounding the secondary air flow into the center region, then a dead zone or a local swirling flow was formed near the wall region as shown in Figures 2 and 15.

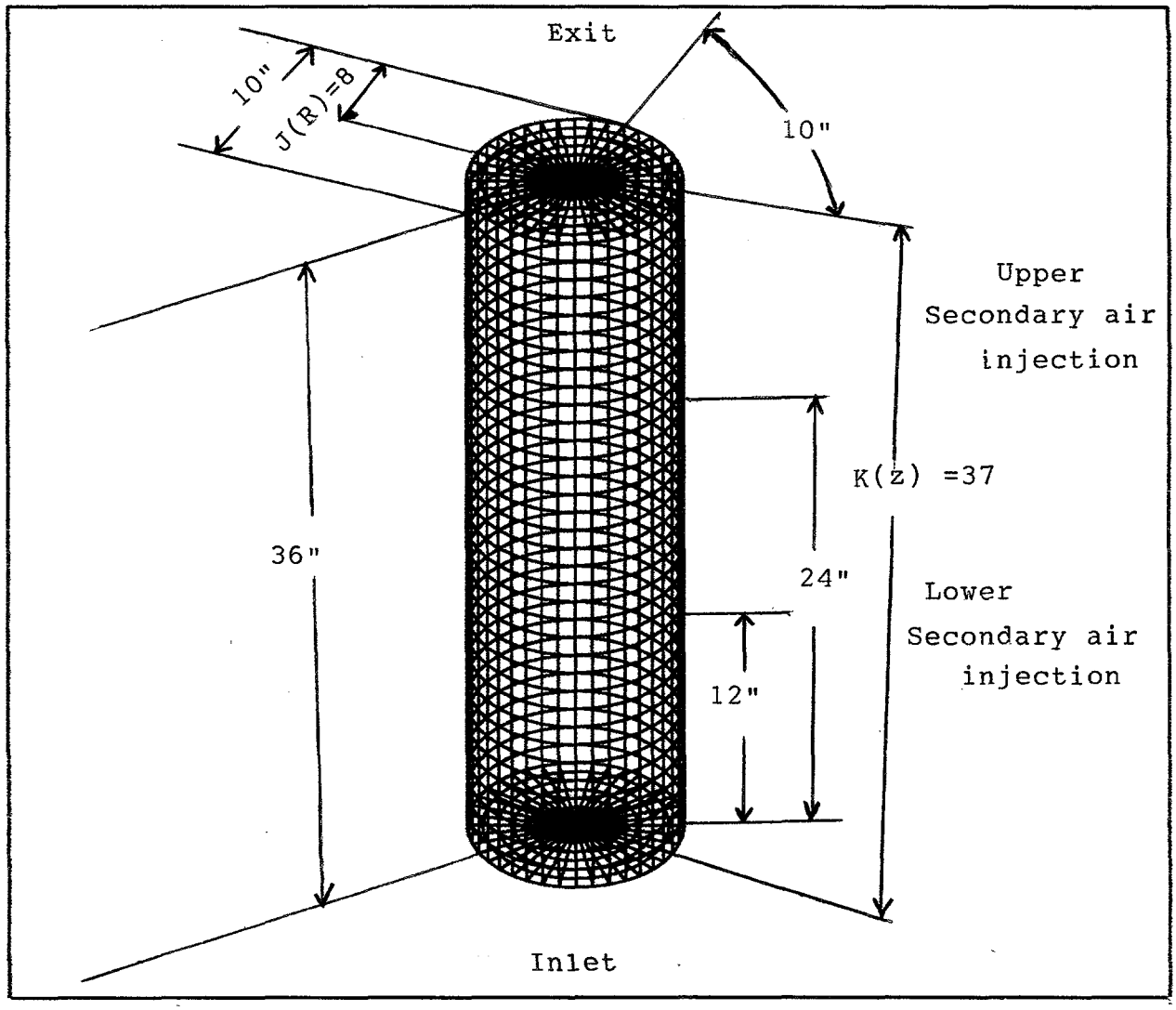

Figure 1 Flow System and Velocity Component in the Freeboard (Slices:K=1, J=8, K=37)

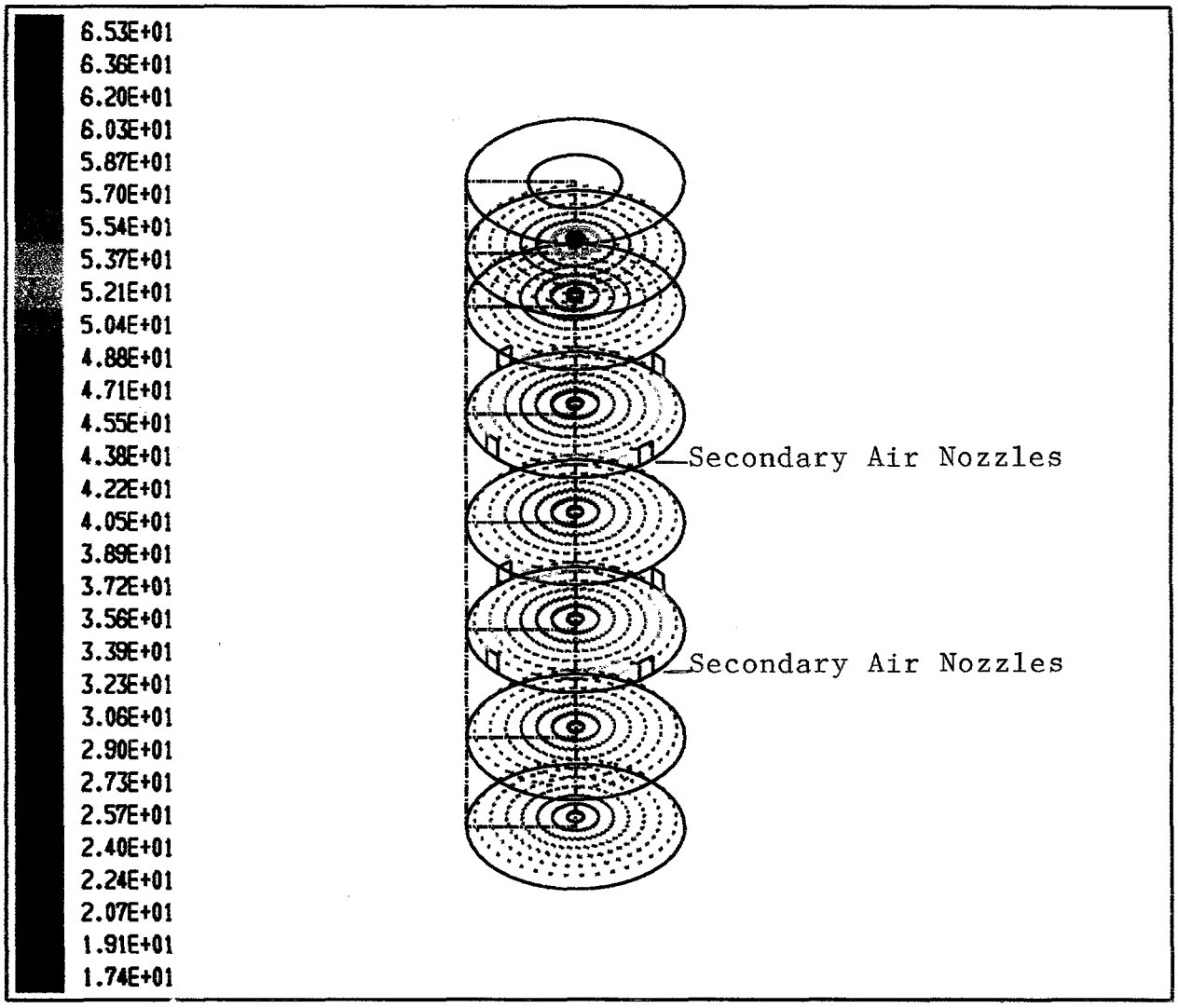

Figure 2 Gas Velocity Vectors (feet/sec)
(K = 1, 6, 12, 24, 18, 24, 30, 33)

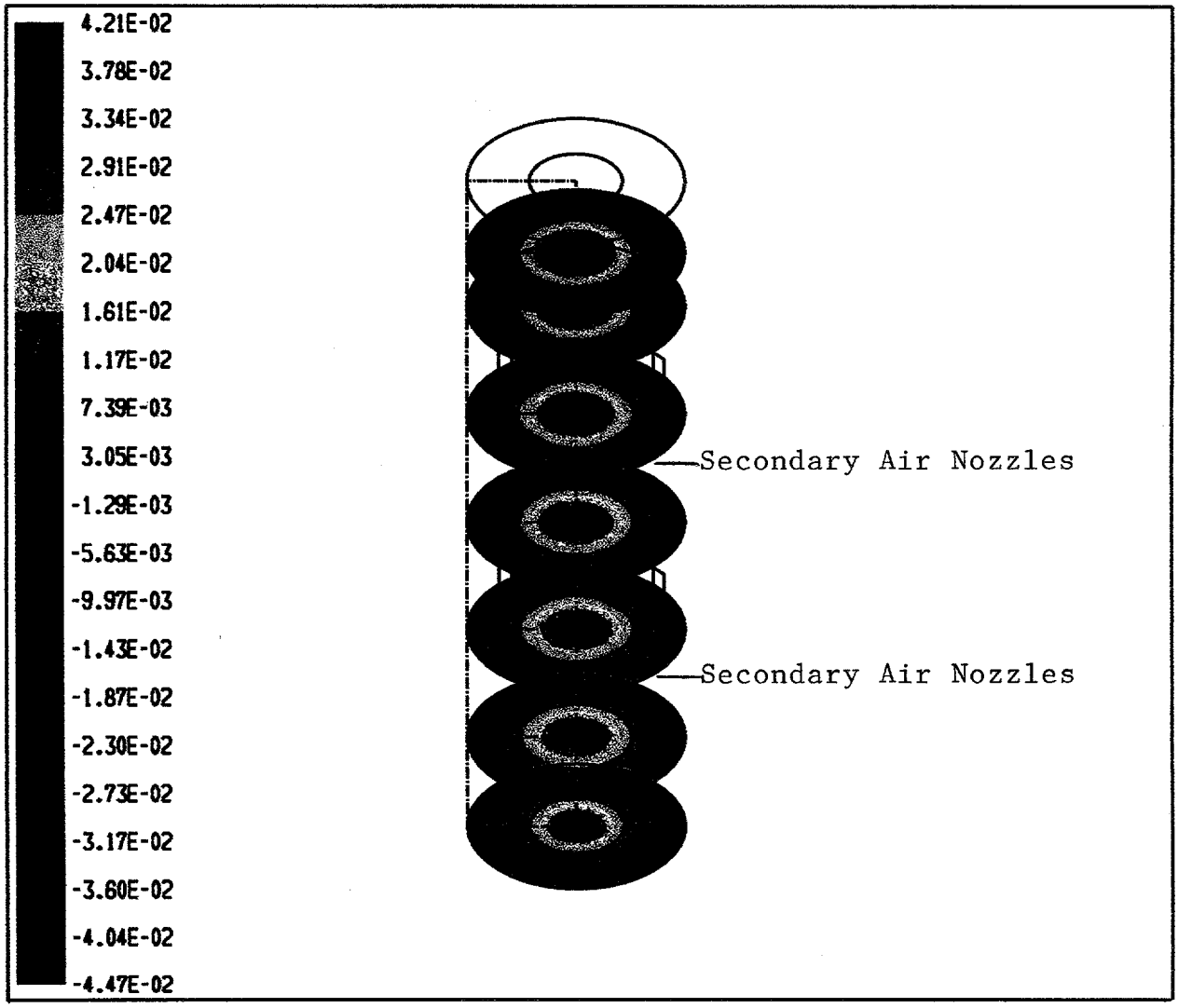

Figure 3 Gas Pressure Profile, Static Pressure (psi)
(K = 1, 6, 12, 18, 24, 30, 33)

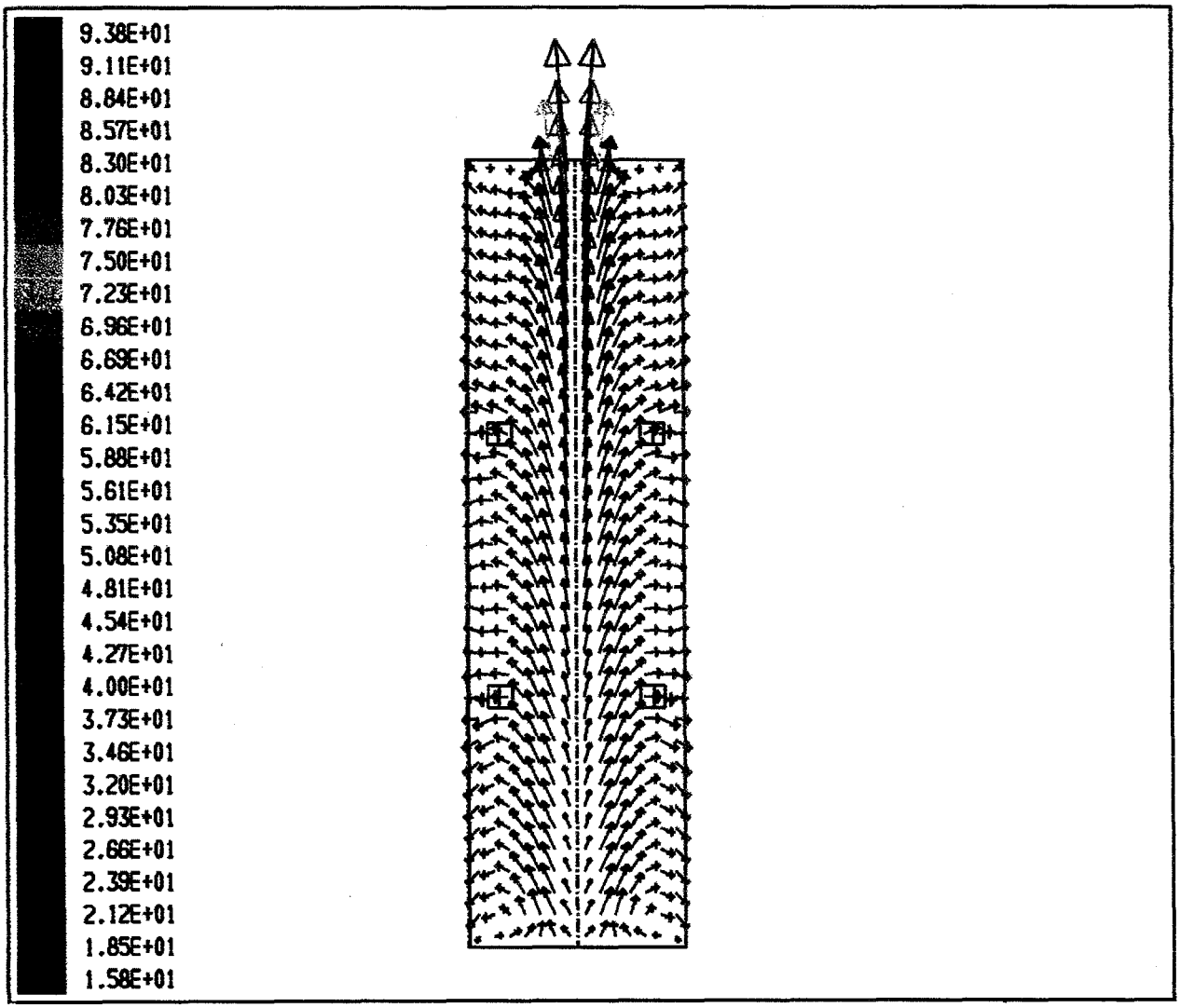

Figure 4 Gas Velocity Vectors(feet/s) with Secondary Air Injection

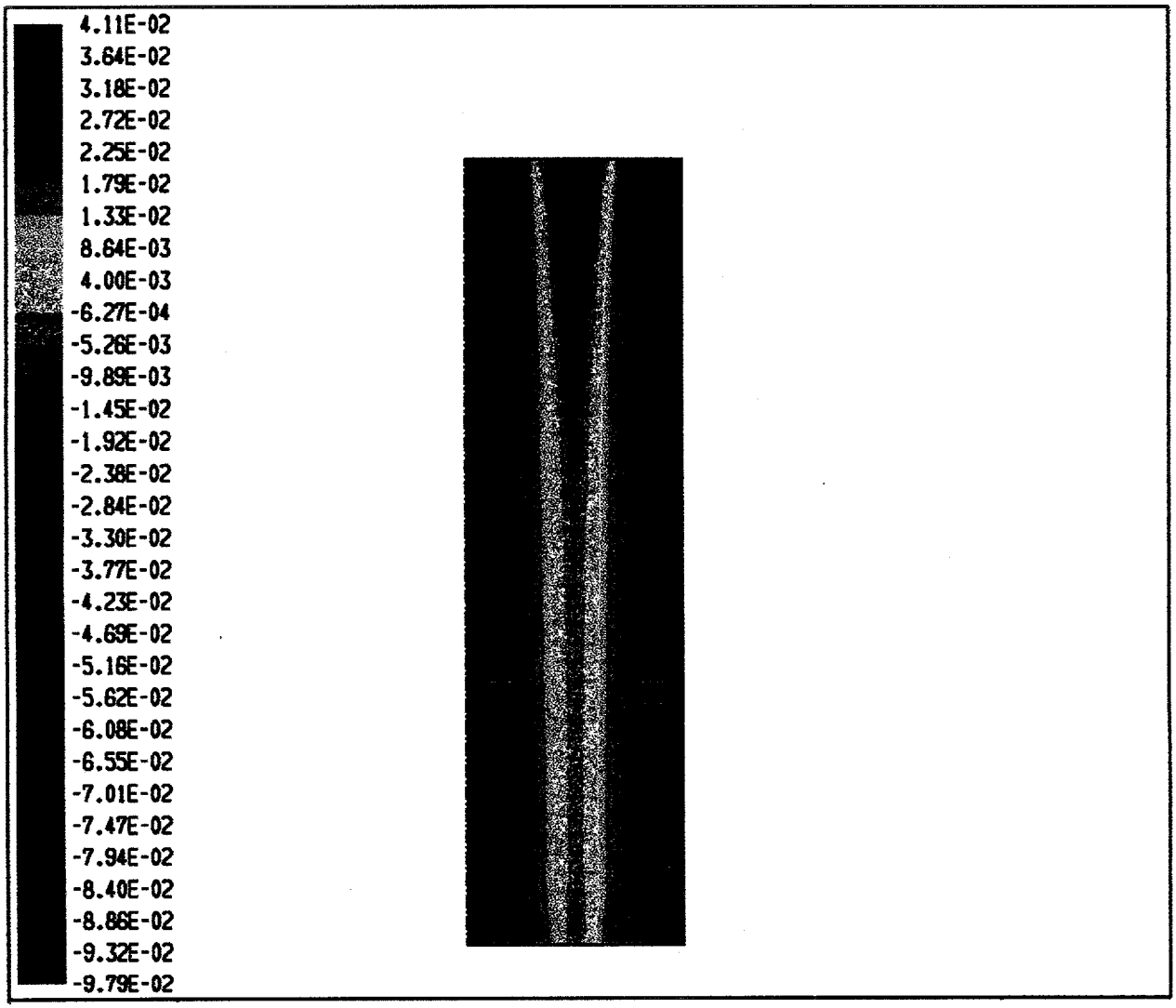

Figure 5 Gas Pressure Profiles (psi)

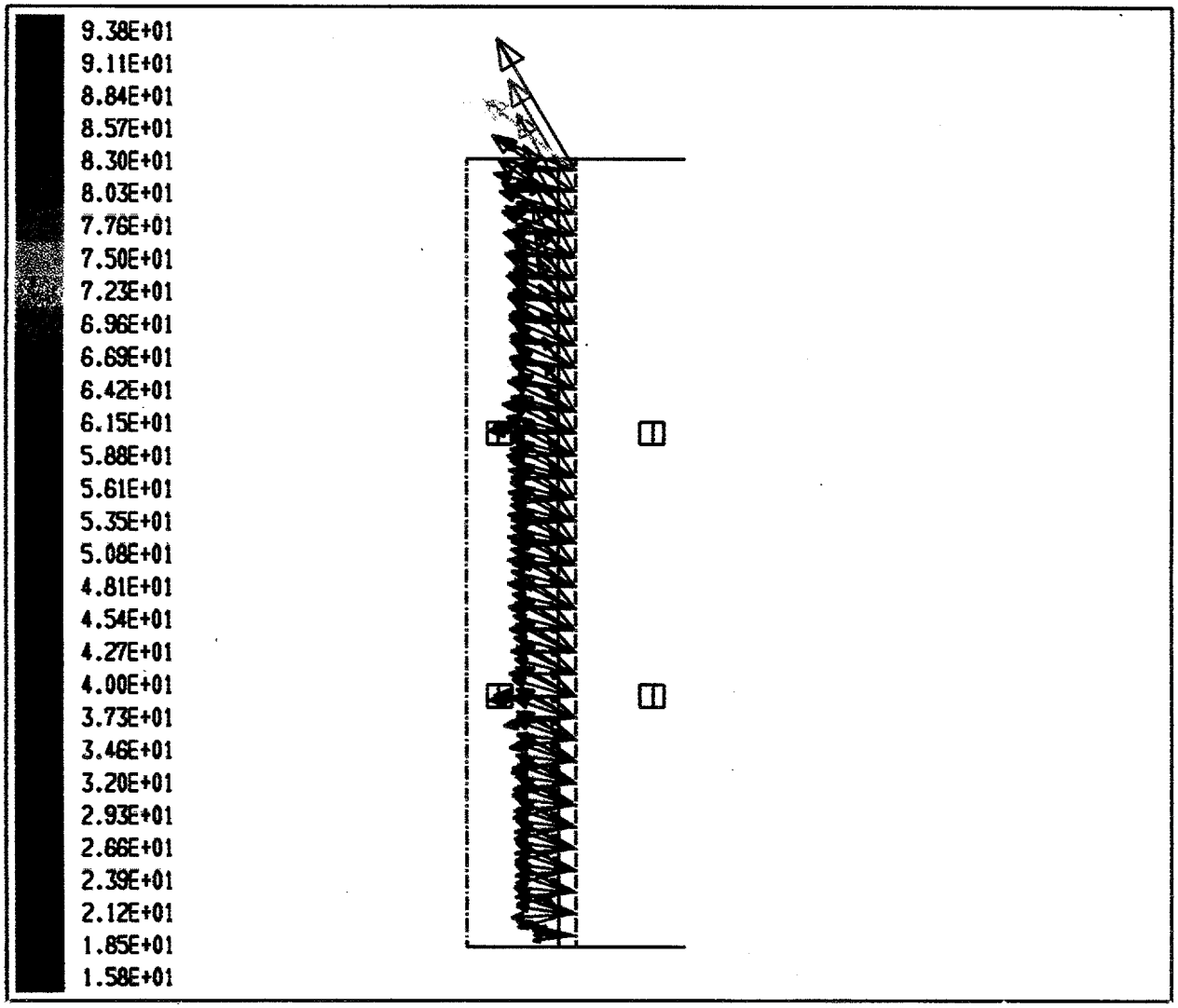

Figure 6 Gas Velocity Vectors (feet/s)

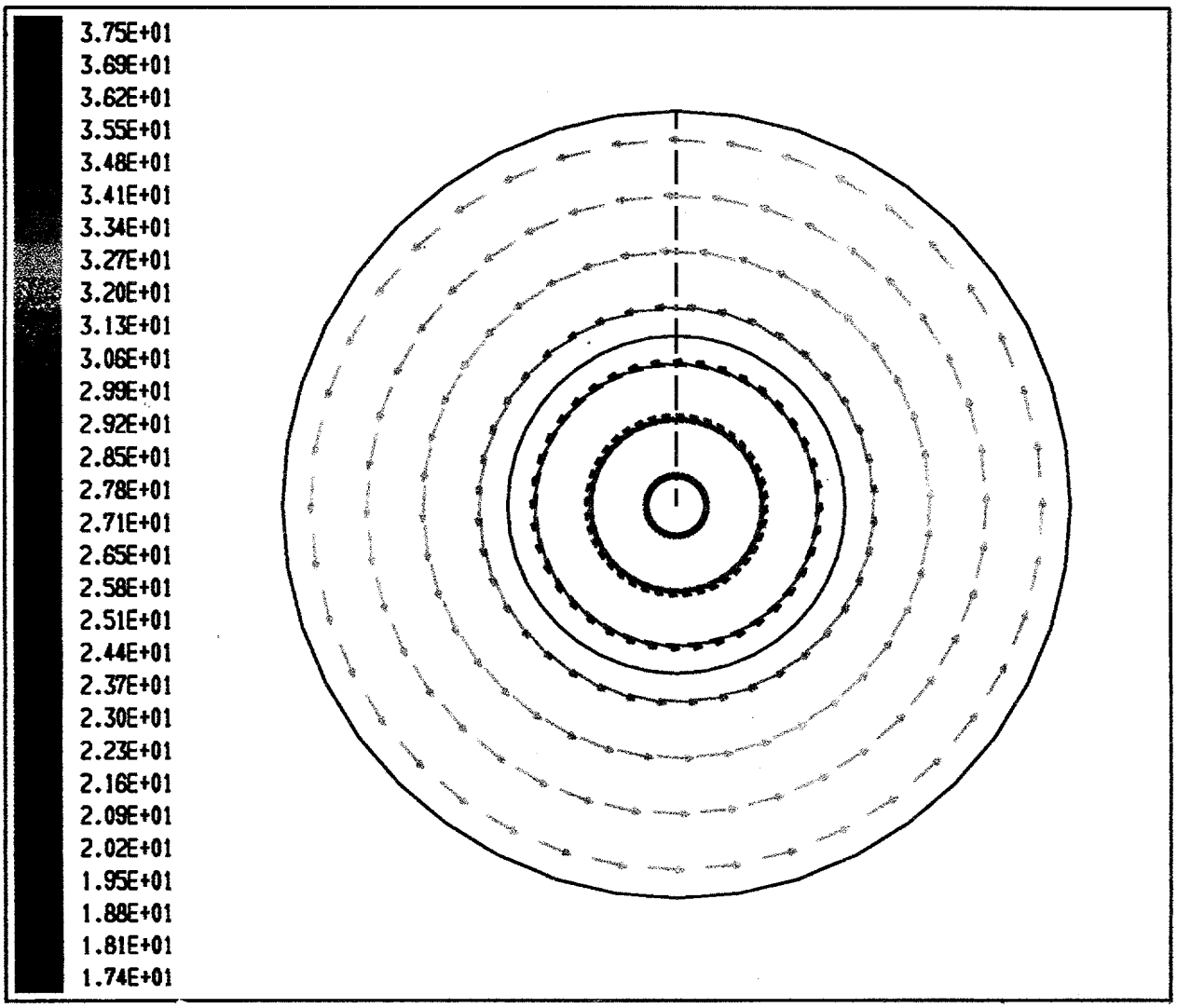

Figure 7 Gas Velocity Vectors (feet/sec)
(K = 6)

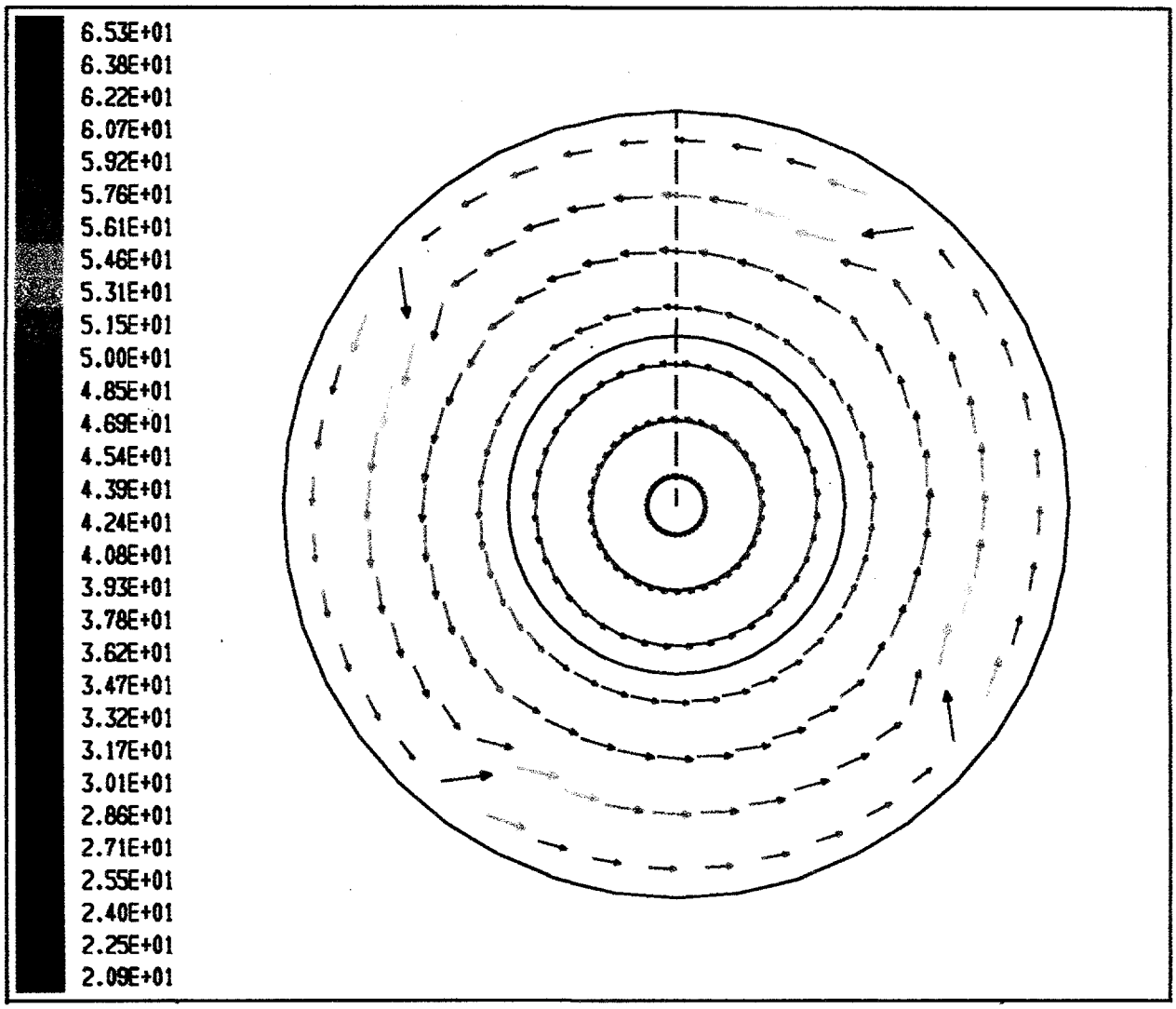

Figure 8 Gas Velocity Vectors (feet/sec)
(K = 12)

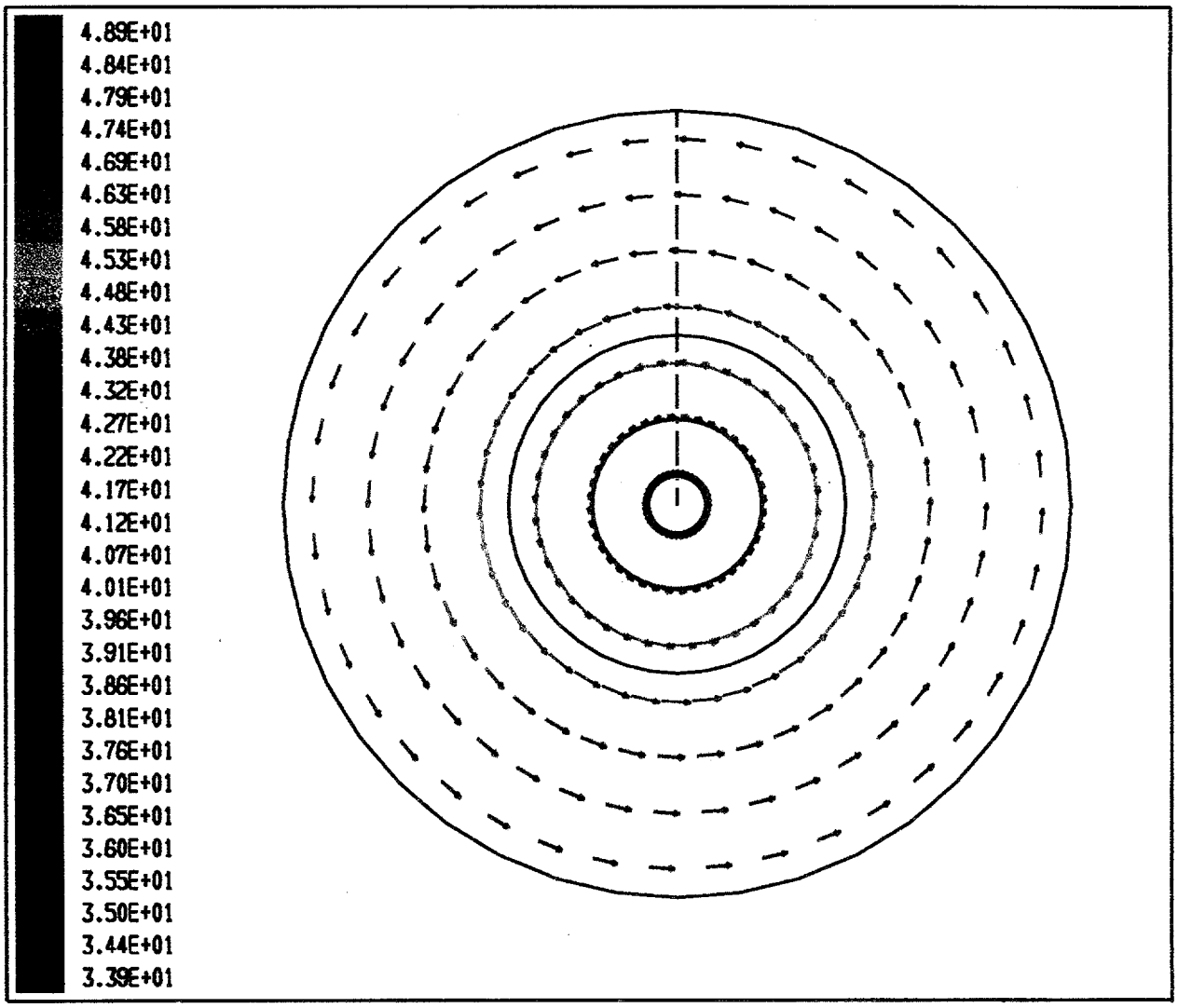

Figure 9 Gas Velocity Vectors (feet/sec)
(K = 18)

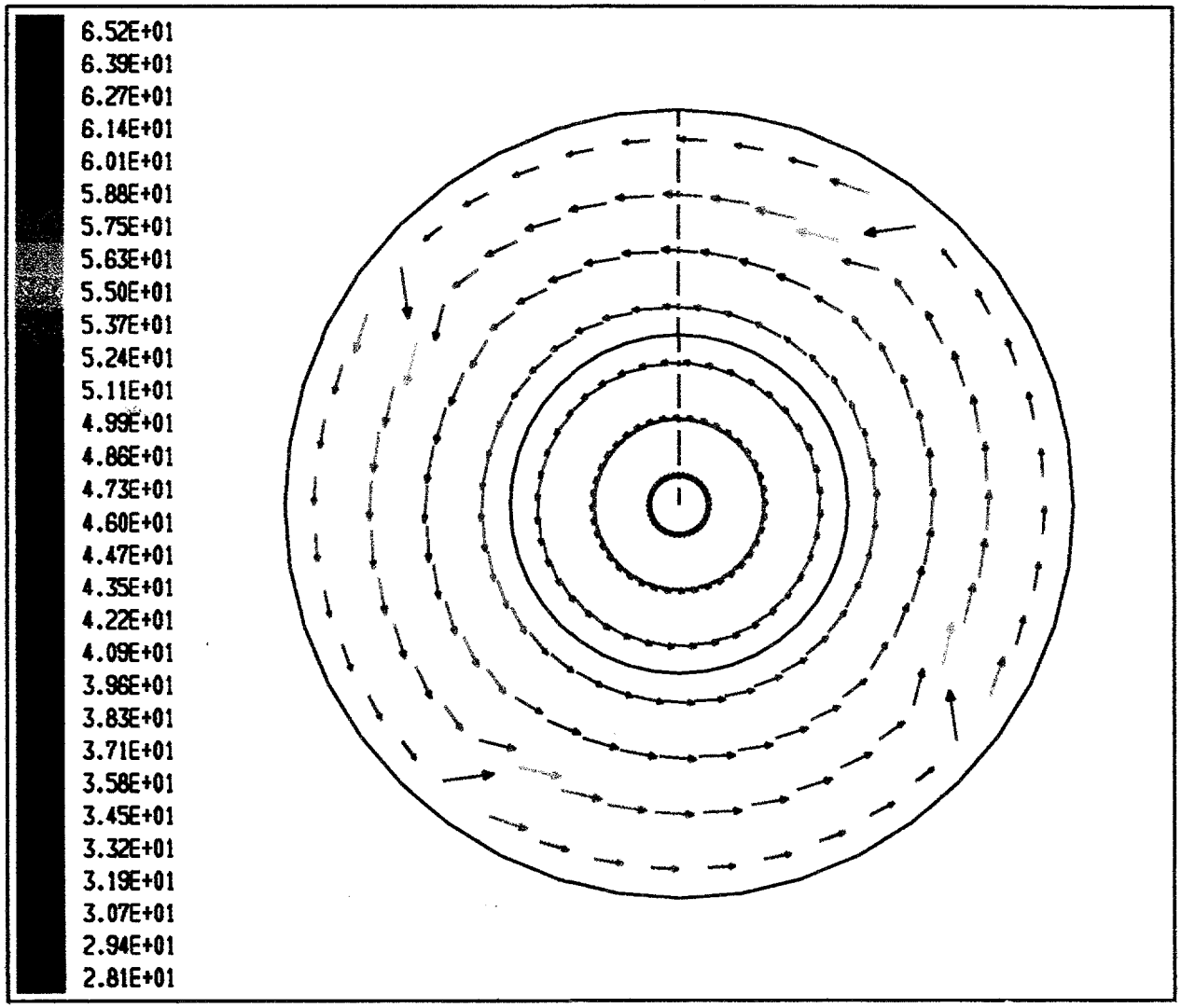

Figure 10 Gas Velocity Vectors (feet/sec)
(K = 24)

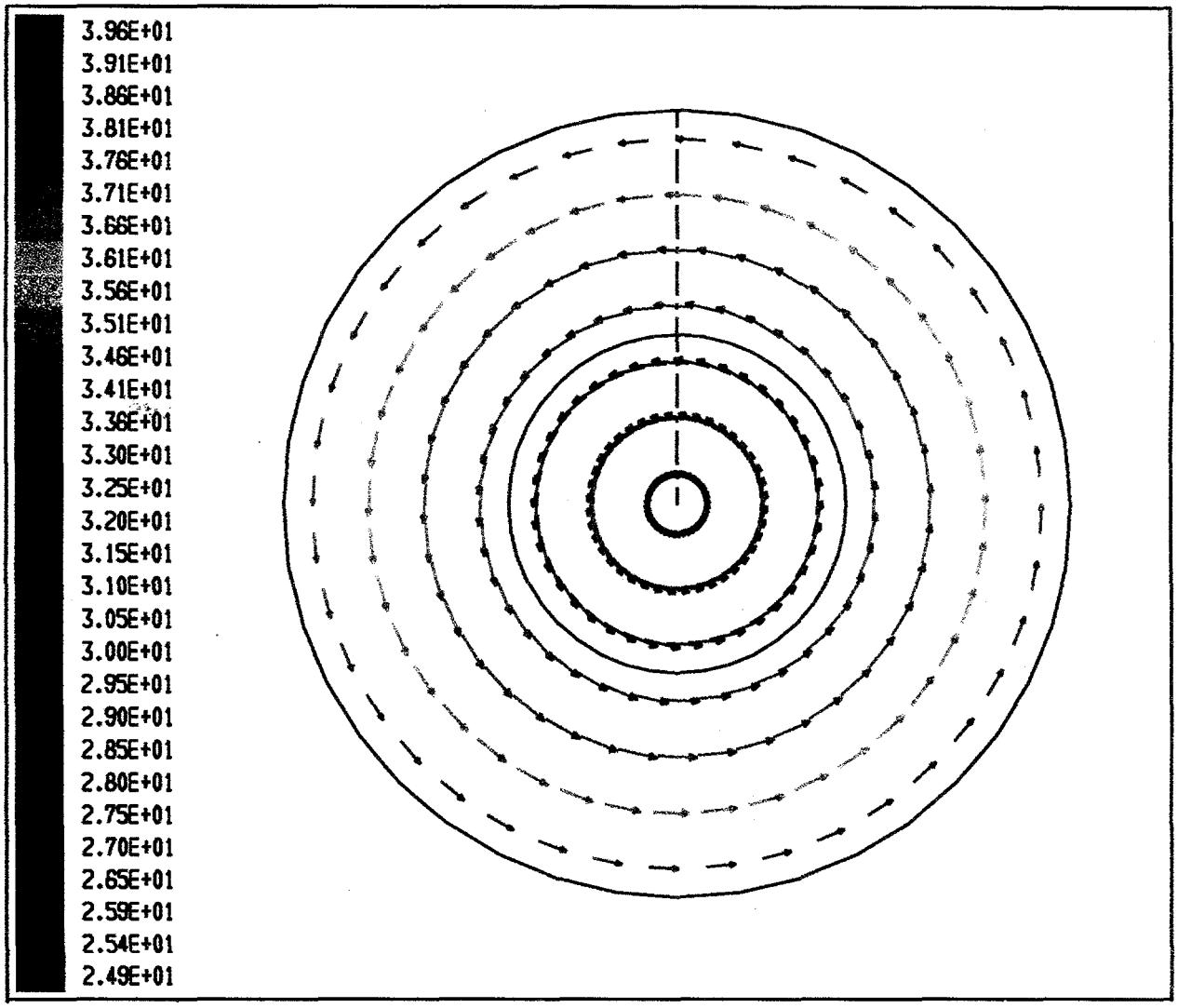

Figure 11 Gas Velocity Vectors (feet/sec)
(K = 30)

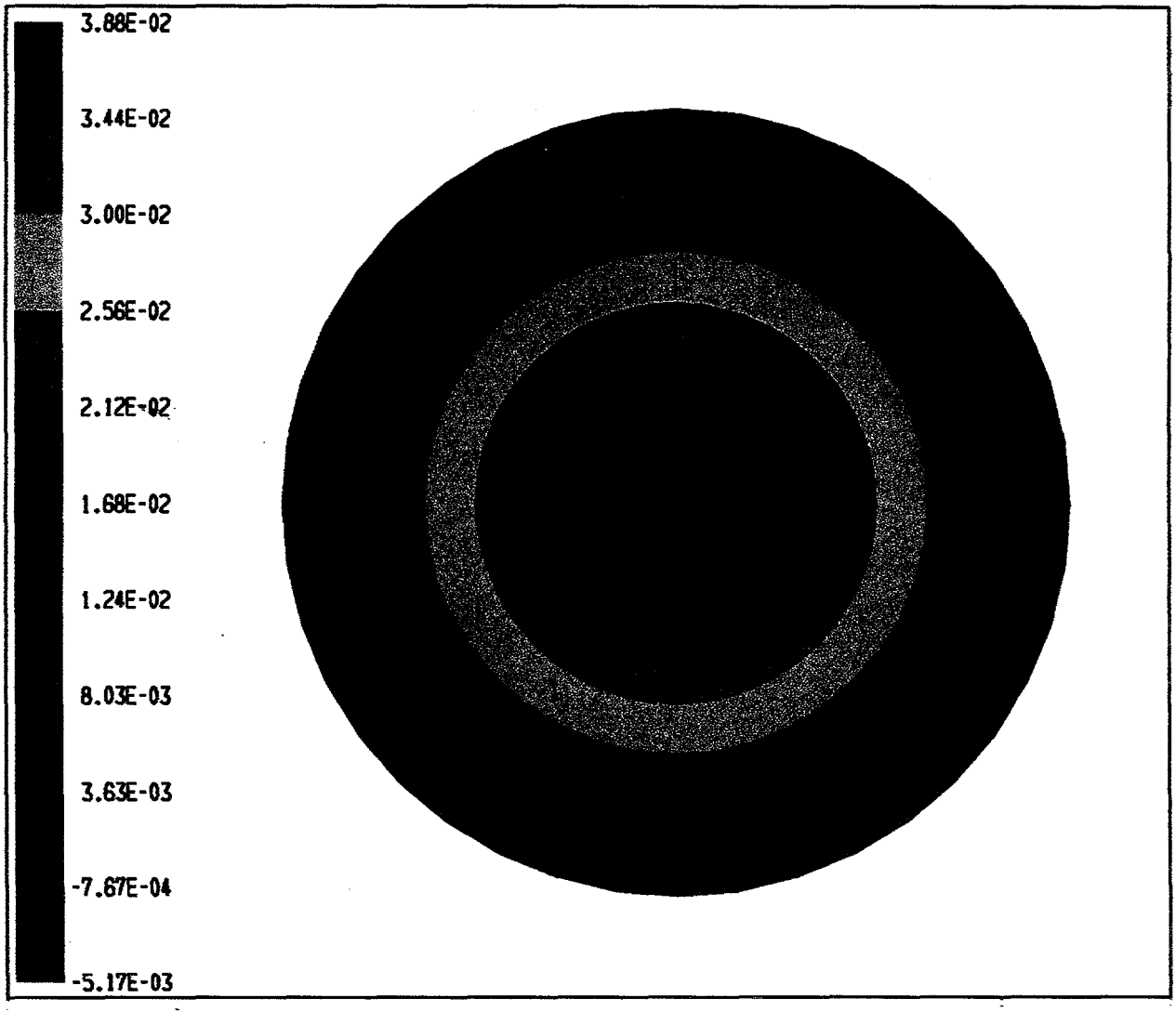

Figure 12 Gas Pressure Profile (psi)
(K = 6)

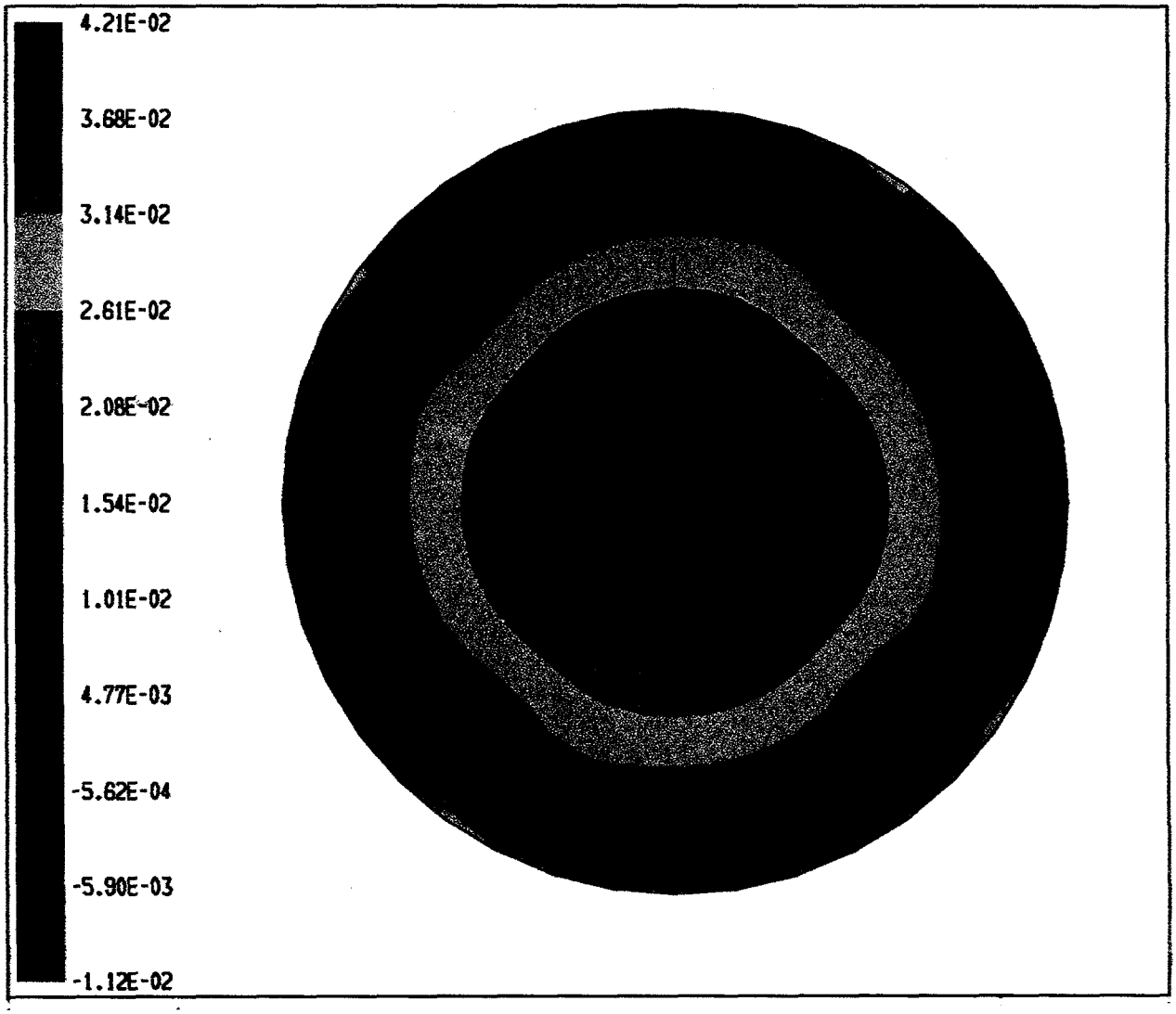

Figure 13 Gas Pressure Profile (psi)
(K = 12)

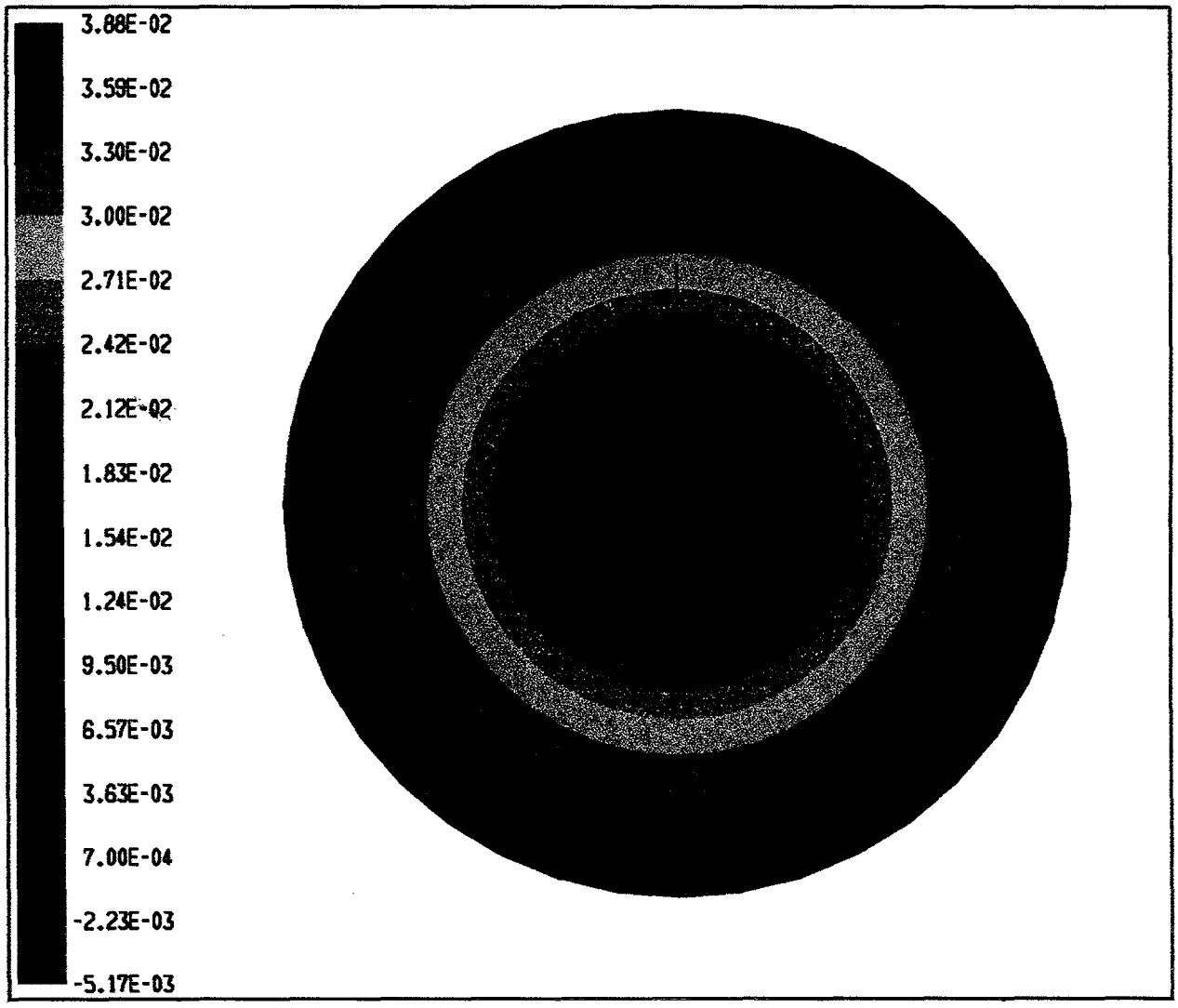

Figure 14 Gas Pressure Profile (psi)
(K = 18)

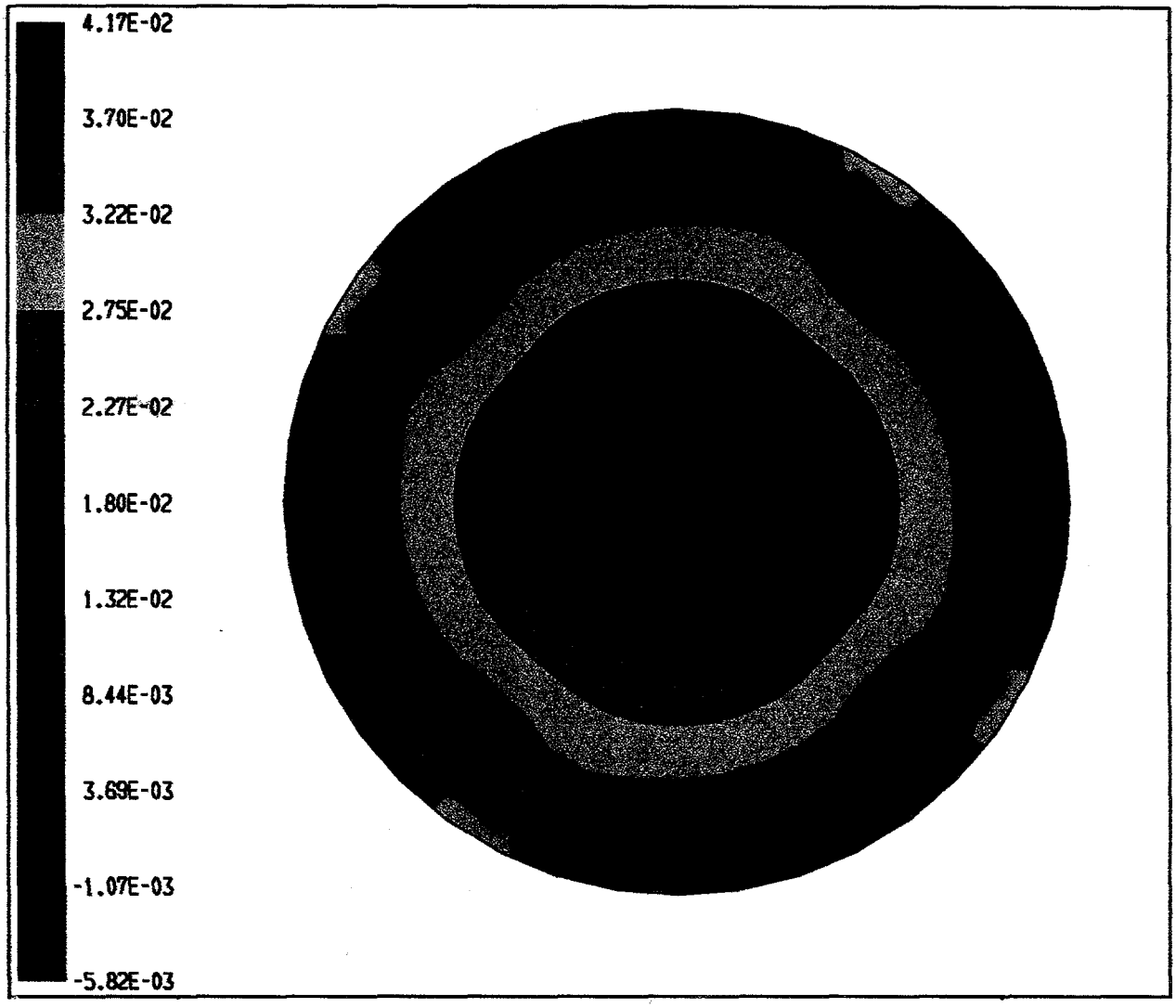

Figure 15 Gas Pressure Profile (psi)
(K = 24)

Section 2

2.1 Design/Fabrication of the Exploratory Hot Model

The exploratory hot model was designed under the situation that understanding of swirling-flow combustion processes was purely based upon theoretical considerations and no relevant technical information except for gas-particle flow characteristics was existent [5].

Figure 2.1 shows the schematic diagram of the combustion chamber and secondary air nozzles. The combustion chamber is made of stainless steel cylinder of 20" height and 9 " diameter, which includes 1" thickness of the refractory line of inside chamber. Heat transfer surfaces, such as water cooling tube, are provided to remove the excess heat and control the combustor temperature to maintain the stable ignition and good burnout of fuels. In addition, heat transfer surfaces assist the turndown operation and turndown ratio.

For our exploratory hot model, the copper tube of 0.5" diameter will be covered to the outside wall of the combustion chamber as the water-cooling tube. Three sections of independently-controlled water-cooling tubes will be arranged to identify the local heat transfer coefficient along the flow directions of the combustion chamber.

Eight secondary air nozzles are arranged with two different levels 6" and 12" respectively from the bottom of the chamber as shown in Figure 2.1. Each level has four nozzles. All of the nozzles have 30 degree yam angle to produce the tangential veloc-

ity. The combustion air will be tangentially injected to the chamber to form a strong swirling, recirculating, turbulent flow field. One of the major design features of the test chamber is strongly swirling flow, which is characterized by the swirl number [6,7]. The calculated swirl number is 12 for this design.

As shown in Figure 2.2, the gas distributor is designed by the flat perforated stainless steel plate. The hole size of the distributor is 0.45" with 152 holes. The gas distributor will be fixed to the bottom flange with 3/8" bolts.

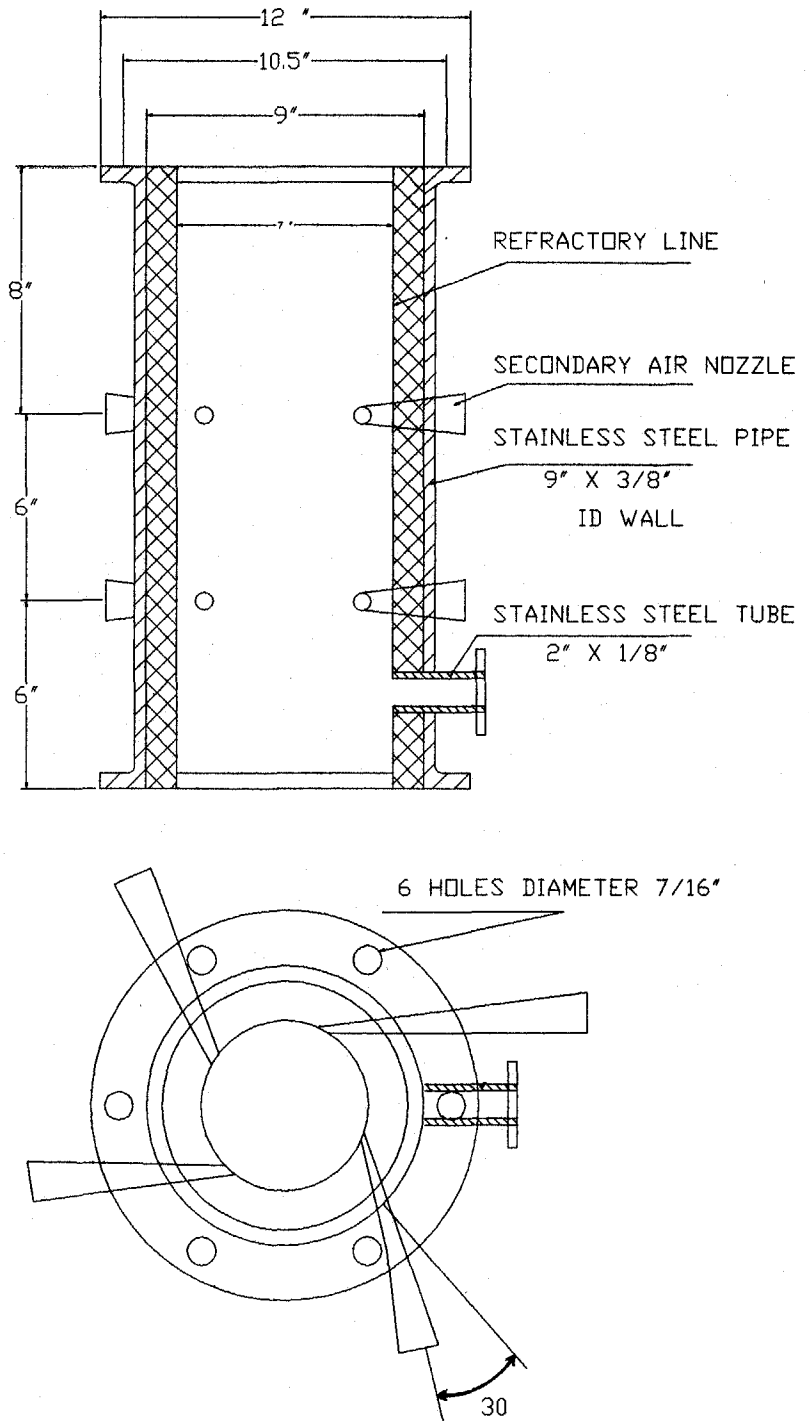

Figure 2.1 Schematic Diagram of the Exploratory Hot Model

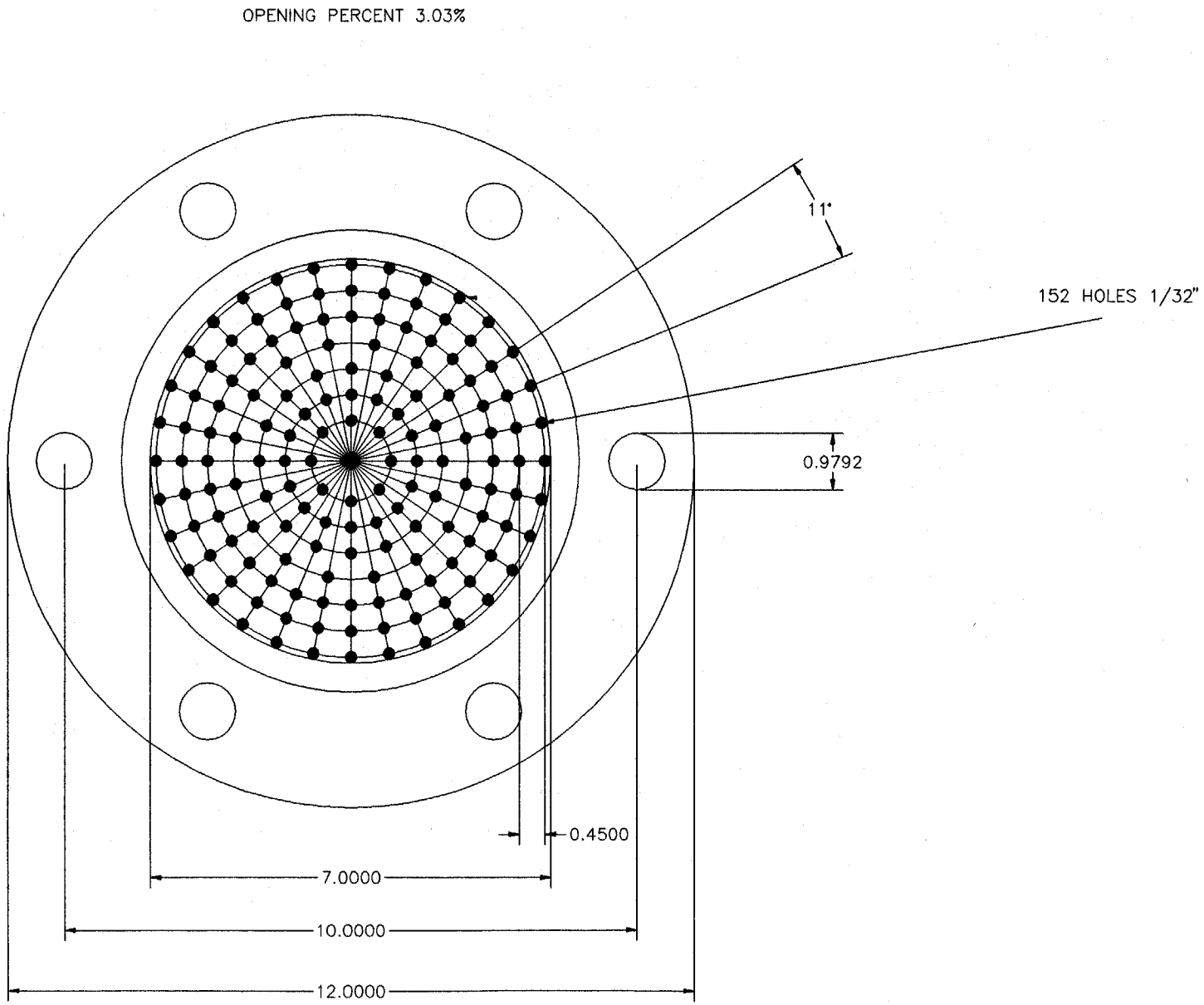

Figure 2.2 Schematic Diagram of the Gas Distributor

REFERENCES

[1] Fluent User's Guide, Vol.4, Chapt. 19, pp. 19/7-19/10, 1995.

[2] Hoffmann, K.A. and S.T. Chiang, Computational Fluid Dynamics, 3rd Ed. Vol.1; Chapt.9, .Vol.2; Chapters 11&13, Engineering Education System, KS, 1995.

[3] Launder, B.E. and D.B. Spalding, Mathematical Models of Turbulence, Academic press, London, 1972.

[4] Boysan, F. and J. Swithenbank, A Fundamental Mathematical Modeling Approach to Cyclone Design, Trans. Inst. Chemical Engineer, V.60, pp.222-230, 1982.

[5] Lee, S.W., Technical Progress Report, Nos. 7, 8, 9, to U.S. DOE, PETC, 1995/1996.

[6] Syred, N. and J.M. Beer, Combustion in Swirling Flows: a Review, Combustion and Flame, Vol.23, pp. 143-201, 1974

[7] Lee, S.W., Technical Progress Report, No. 5 to U.S. DOE PETC, January 1995.